Manuscript prepared for Clim. Past
with version 2015/04/24 7.83 Copernicus papers of the LaTeX class copernicus.cls.
Date: 1 April 2016

The link between marine sediment records and changes in Holocene Saharan landscape: simulating the dust cycle

Sabine Egerer [1,2], Martin Claussen [1,3], Christian Reick [1], and Tanja Stanelle [4]

[1]Max Planck Institute for Meteorology, Bundesstraße 53, 20146 Hamburg, Germany
[2]International Max Planck Research School on Earth System Modelling, Bundesstraße 53, 20146 Hamburg, Germany
[3]Center for Earth System Research and Sustainability, Universität Hamburg, Bundesstraße 53, 20146 Hamburg, Germany
[4]Center for Climate System Modeling, ETH Zurich, Universitaetstrasse 16, 8092 Zurich, Switzerland

Correspondence to: Sabine Egerer (Sabine.Egerer@mpimet.mpg.de)

Abstract.

Marine sediment records reveal an abrupt and strong increase in dust deposition in the North Atlantic at the end of the African Humid Period about 4.9 ka to 5.5 ka ago. The change in dust flux has been attributed to varying Saharan land surface cover. Alternatively, the enhanced dust accumulation is linked to enhanced surface winds and a consequent intensification of coastal upwelling. Here we demonstrate for the first time the direct link between dust accumulation in marine cores and changes in Saharan land surface. We simulate the mid-Holocene (6 ka BP) and pre-industrial (1850 AD) dust cycle as a function of Saharan land surface cover and atmosphere-ocean conditions using the coupled atmosphere-aerosol model ECHAM6.1-HAM2.1. Mid-Holocene surface characteristics, including vegetation cover and lake surface area, are derived from proxy data and simulations. In agreement with data from marine sediment cores, our simulations show that mid-Holocene dust deposition fluxes in the North Atlantic were two to three times lower compared with pre-industrial fluxes. We identify Saharan land surface characteristics to be the main control on dust transport from North Africa to the North Atlantic. We conclude that the increase in dust accumulation in marine cores is directly linked to a transition of the Saharan landscape during the Holocene and not due to changes in atmospheric or ocean conditions alone.

1 Introduction

The transition from the 'green' Sahara of the early to mid-Holocene, about 9 to 6 ka BP, to today's hyperarid conditions was triggered by a steady shift in orbital forcing. The Northern hemisphere received in average about 4.5% more summer insolation during the early to mid-Holocene compared to present times (Berger, 1978) causing a higher temperature gradient between the North African

subcontinent and the Eastern Atlantic Ocean prior to monsoon onset in late spring. This led to a strengthening of the West African summer monsoon and a consequent northward shift of the West African rain belt (Kutzbach, 1981). A wet climate supported the establishment of permanent vegetation cover and lakes in the area of today's hyperarid Sahara (Kutzbach and Street-Perrott, 1985; Jolly et al., 1998; Kohfeld and Harrison, 2000). Pollen records indicate a considerable expansion of vegetation in North Africa north of 15°N at that time (Prentice et al., 2000) with steppe, savanna and temperate xerophytic woods and shrubs extending up to 23°N (Jolly et al., 1998). Lakes and wetlands were widespread up to 30°N and covered about 7.6% of North Africa (Street-Perrott et al., 1989; Hoelzmann et al., 1998; Jolly et al., 1998; Kröpelin et al., 2008). The largest water body was lake Mega-Chad with an area of at least 350 000 km^2 presumably (Schuster et al., 2005).

Marine sediment cores along the northwest African margin reveal an abrupt and strong increase in dust accumulation in the North Atlantic of about 140% some 5.5 ka ago (Adkins et al., 2006) up to a factor of 5 about 4.9 $\pm$ 0.2 ka BP (McGee et al., 2013). The change in dust flux has been attributed to varying Saharan vegetation cover predicted by Brovkin et al. (1998) and Claussen et al. (1999) or was related to a change in lake surface area (Cockerton et al., 2014; Armitage et al., 2015). Alternatively, the enhanced dust accumulation is linked to enhanced surface winds and a consequent intensification of coastal upwelling (Adkins et al., 2006; Bradtmiller et al., 2016). However, until now no modeling study exists that explicitly simulated the mid-Holocene dust cycle to explore the link between Saharan land surface cover and North Atlantic dust deposits at the particular location of the marine cores.

Two modeling studies of the dust cycle using general circulation models (GCMs) cover the mid-Holocene era. Albani et al. (2015) performed simulations of a 6 ka BP and a pre-industrial time slice using the Community Earth System Model (CESM) including a Bulk Aerosol Model (CAM4-BAM). Vegetation was set to pre-industrial conditions according to PMIP/CMIP prescriptions for both time slices. The soil erodibility was scaled for each grid cell based on vegetation cover, which was obtained offline by BIOME4 simulations. Sudarchikova et al. (2015) simulated the global dust cycle for several time slices including pre-industrial and mid-Holocene with focus on Antarctica using the ECHAM5-HAM model. Paleoclimatic vegetation was simulated with the dynamic vegetation model LPJ-GUESS. They obtained a similar fractional vegetation cover distribution in North Africa for mid-Holocene and pre-industrial, what is in contradiction with paleorecords that specify extensive vegetation indicating a much higher vegetation cover fraction between 15°N and 23°N (Hoelzmann et al., 1998; Jolly et al., 1998). As sparse or non-vegetated areas are potential dust sources, Saharan dust emission was thus overestimated for the mid-Holocene (results for North African dust emission presented in Sudarchikova (2012)). The extent of paleolakes was not taken into account in either study, despite the fact that areas covered by lakes lose their potential as a dust source. Accordingly, marine sediment records along the northwest African margin (deMenocal et al., 2000; Adkins et al., 2006; McGee et al., 2013; Albani et al., 2015) indicate a lower dust accumulation rate and less

dust emission in North Africa than suggested in the modeling studies. Also in Albani et al. (2015), deviations between modeled and observed dust depositions in the North Atlantic could arise from an underestimation of vegetation cover as models typically fail to capture mid-Holocene vegetation cover as indicated by proxies (Hoelzmann et al., 1998) to its full extent (Doherty et al., 2000; Irizarry-Ortiz et al., 2003; Rachmayani et al., 2015).

To overcome the shortcomings of previous simulation studies on the mid-Holocene dust cycle, we account for a more realistic land surface cover. We prescribe mid-Holocene vegetation conditions in North Africa based on reconstructions of Hoelzmann et al. (1998) and specify the distribution of paleolakes from simulations (Tegen et al., 2002). We investigate Holocene dust emission, transport and deposition explicitly as a function of Saharan land surface characteristics and atmosphere-ocean conditions. To quantify changes in marine dust deposition, we perform equilibrium simulations of the mid-Holocene ($6k$) and pre-industrial ($0k$) dust cycle using the coupled climate-aerosol model ECHAM6.1-HAM2.1. The investigations are guided by the following questions: Can we support the interpretation of enhanced dust accumulation seen in the marine sediment cores as a consequence of changes in North African landscape? Or can already changes in atmosphere-ocean conditions alone explain these observations? Technically, we separate the importance of land surface and atmosphere-ocean conditions on dust emission and deposition following the factor separation method of Stein and Alpert (1993).

In section 2, the model and the experimental setup is described and the factor separation method is introduced briefly. The model is evaluated by comparing present day global dust emission quantitatively and qualitatively with the AEROCOM Intercomparison study (Huneeus et al., 2011). Results are presented in section 3. Simulated mid-Holocene and pre-industrial dust deposition rates are compared to those indicated from marine sediment records along the northwest African margin. The influence and weighting of land surface and atmosphere-ocean conditions is determined applying a factor analysis method. A discussion of the results, conclusions and suggestions for future studies follow in section 4.

2 Methodology

2.1 Model description

We employ the comprehensive climate-aerosol model ECHAM-HAM (echam6.1.0-ham2.1-moz0.8) (Stier et al., 2005; Zhang et al., 2012) at a model resolution of T63L31 corresponding to a horizontal resolution of approximately 1.9°x1.9° and 31 vertical (hybrid)sigma-pressure levels in the atmosphere. The aerosols included in the model are mineral dust, sulfate, black carbon, organic carbon and sea salt. The aerosol concentrations from natural sources are calculated interactively in the model. In the analysis, we focus only on mineral dust.

We use a model version equivalent to Stanelle et al. (2014) where the standard version is extended to determine potential dust source areas directly depending on land surface cover. Bare soil regions or areas that are covered by sparse vegetation such as grass, shrubs or crops are potential source regions. The role of exposed paleolake beds as preferential sources of dust under dry conditions is accounted for in the model. The surface material deposited in the paleolake basins is assumed to consist of silt-sized aggregates, which makes them a highly productive source of dust (Tegen et al., 2002). Dust particles are emitted from preferential and potential source regions if specific criteria are fulfilled, e.g. the wind velocity has to exceed a threshold, the soil is not covered by snow, the upper soil layer has to be dry.

The amount of emitted aeolian dust areas is calculated following Tegen et al. (2002). Dust particles are grouped in 192 dust size classes with diameters ranging from 0.2 to 1300 μm. After exceeding a threshold friction wind velocity, that is specific for each size class and depends on soil moisture and texture, dust fluxes increase nonlinearly as a function of wind velocity. The explicit formulation of the calculation of horizontal fluxes follows Marticorena and Bergametti (1995). The main mechanism considered in the scheme is saltation bombardment. The ratio between vertical and horizontal emission fluxes is prescribed for different soil types based on empirical measurements and depends on particle size distribution and surface properties (Marticorena et al., 1997). Soil types are clay, silt, medium/fine sand and coarse sand (Tegen et al., 2002). Vertical emission fluxes are then integrated over all size classes and divided into aerosol modes, for which log-normal distributions are prescribed: accumulation mode (mass mean radius (mmr)=0.37 μm, standard derivation σ=1.59 μm) and coarse mode (mass mean radius (mmr)=1.75 μm, standard derivation σ=2 μm). Emission into the super-coarse mode is neglected because of the short life time of particles. Aerosol transport and interaction with the atmosphere is calculated according to Stier et al. (2005). Dust is removed from the atmosphere via dry deposition, wet deposition or sedimentation.

2.2 Model validation

Within the framework of the AEROCOM global dust model intercomparison project, the results of several global aerosols models are compared to observations to detect uncertainties and shortcomings

in the simulation of the global dust cycle under present day climate (Huneeus et al., 2011). There still remain large uncertainties in modeling the global dust cycle. Among the models, simulated dust emission, deposition and the atmospheric burden vary by about an order of magnitude, for example emissions in North Africa range from 204 to 2888 Tga^{-1}.

A detailed evaluation of the current model version is presented by (Stanelle et al., 2014). Emission and deposition fluxes as well as the atmospheric burden are within the range of the AEROCOM results for ECHAM6.1-HAM2.1 for present day climate, but results of the ECHAM-HAM model are found to be lower than the AEROCOM median in general (see their Table 1).

2.3 Experimental setup

We perform equilibrium simulations to study the mid-Holocene ($6k$) and pre-industrial ($0k$) global dust cycle. The main setup is composed of four experiments (Table 2) to 1) compare with marine sediment records for both $6k$ and $0k$ (section 3.1) and 2) identify the drivers of a change in dust flux between $6k$ and $0k$ (section 3.2). We separate two factors: a) Saharan land surface conditions (vegetation cover and lake surface area) and b) atmosphere-ocean conditions including orbital forcing, sea surface temperature (SST) and sea ice cover (SIC).

AO refers to atmosphere and ocean conditions. Orbital parameters are adapted to $0k$ and $6k$ respectively following Berger (1978) (Table 3). Prescribed SST and SIC for the pre-industrial era and the mid-Holocene respectively are taken from CMIP5 simulations with MPI-ESM (Giorgetta et al., 2013). The setup is defined following the CMIP5 protocol (Taylor et al., 2011). LV defines land surface conditions including lake and vegetation cover. Mid-Holocene vegetation cover reconstruction in North Africa (17°W - 40°E; 10°N - 30°N) is based on a vegetation map of Hoelzmann et al. (1998). In their approach, pollen data is linked to corresponding biomes; roughly, savanna vegetation is assumed between 10°N and 20°N and steppe vegetation between 20°N and 30°N. In the land surface component JSBACH of ECHAM, biomes are represented as a composition of plant functional types (PFT). Vegetation fraction and cover fractions of all eleven PFTs, surface albedo and water conductivity are set accordingly. Steppe is linked to C4 grasses and a vegetation cover of 58%. Savanna is composed of 80% C4 grasses and 20% tropical evergreen forest, where vegetation covers 80% of the land (Hagemann, 2002). Although the absolute vegetation fraction and the cover fractions of the PFTs are fixed, the leaf area index (LAI) is calculated interactively based on changes in net primary productivity (NPP) during the seasonal cycle. In JSBACH, a standard vegetation map for pre-industrial conditions was derived from Hagemann (2002) using satellite data. Pre-industrial and reconstructed mid-Holocene vegetation fraction are shown in Fig. 1. During the mid-Holocene the extent of lakes was much more pronounced than it is today (Hoelzmann et al., 1998; Gasse, 2000). Thus, the fractional lake mask in the model is adapted to a reconstruction of paleolakes from Tegen et al. (2002). They calculated the maximum possible lake extent by filling up closed topo-

graphic basins using a high-resolution water routing and storage model (see Fig. 1 for $0k$ and $6k$ lake fraction).

In addition to the main simulations, we perform two simulations to separate the effect of altering vegetation and lake cover under mid-Holocene atmosphere-ocean conditions. In the fifth simulation, $AO_{6k}L_{0k}V_{6k}$, mid-Holocene vegetation is set and paleolakes are dried out. In the sixth simulation, $AO_{6k}L_{6k}V_{0k}$, only paleolakes are considered, whereas vegetation cover is set to the pre-industrial state (Table 2).

Each simulation is run for 31 years including one year of spin-up time. Thus, all results refer to an average of 30 years. The $6k$ setup, including orbital forcing parameters and greenhouse gases, is following the PMIP project standards (Harrison et al. (2001); Table 3). $0k$ and $6k$ greenhouse gas concentrations of CO_2, CH_4 and N_2O are set equally to $6k$ values of the PMIP protocol. The control run is denoted by $AO_{0k}LV_{0k}$.

2.4 Factor separation

To isolate the impacts of a) land surface conditions and b) atmosphere-ocean conditions on dust emission in North Africa and deposition fluxes in the North Atlantic along the northwest African margin, we apply the factor separation method of Stein and Alpert (1993) to the four main simulations $AO_{0k}LV_{0k}$, $AO_{6k}LV_{0k}$, $AO_{0k}LV_{6k}$ and $AO_{6k}LV_{6k}$. We explain the methodology exemplified for dust emission. The amount of emitted dust in North Africa is

$$f(s) = \int_{10^\circ N}^{30^\circ N} \int_{17^\circ W}^{40^\circ E} e_s(x,y)dxdy, \qquad s \in \{AO_{0k}LV_{0k}, AO_{6k}LV_{0k}, AO_{0k}LV_{6k}, AO_{6k}LV_{6k}\} \tag{1}$$

where $e_s(x,y)$ is the simulated dust emission at point (x,y) for simulation s.

The total difference in dust emission in North Africa between $6k$ and $0k$

$$\Delta_{6k-0k} = f(AO_{6k}LV_{6k}) - f(AO_{0k}LV_{0k}) \tag{2}$$

is divided into three components

$$\Delta_{6k-0k} = \Delta_{AO} + \Delta_{LV} + \Delta_{SYN}. \tag{3}$$

The contribution Δ_{AO} due to differences in orbital forcing, SST and SIC and the contribution Δ_{LV}, which captures the effects of changed land surface cover, are given by

$$\Delta_{AO} = f(AO_{6k}LV_{0k}) - f(AO_{0k}LV_{0k}), \tag{4}$$

$$\Delta_{LV} = f(AO_{0k}LV_{6k}) - f(AO_{0k}LV_{0k}). \tag{5}$$

The synergy between both factors reads

$$\Delta_{SYN} = f(AO_{6k}LV_{6k}) - f(AO_{0k}LV_{0k}) - (\Delta_{AO} + \Delta_{LV}) \tag{6}$$

$$= f(AO_{6k}LV_{6k}) - f(AO_{6k}LV_{0k}) - f(AO_{0k}LV_{6k}) + f(AO_{0k}LV_{0k}). \tag{7}$$

3 Results

We find the Sahara and especially the dry non-vegetated areas in Western Africa and the Bodélé Depression in the central Sahara to provide some of the most productive dust sources worldwide (Fig. 2), which is in agreement with satellite data (Middleton and Goudie, 2001; Engelstaedter and Washington, 2007). The patterns of deviations in dust emission between the $6k$ simulation and the pre-industrial control are clearly related to differences in lake patterns (Fig. 1), e.g. lake Mega-Chad covered the area where we find the Bodélé Depression today (Schuster et al., 2005). Also in West Africa smaller lakes and wetlands were widespread preventing dust emission.

While land surface conditions were modified solely in North Africa, we notice a small area with changing dust emission in the south of the Arabian peninsula and dust depositions expanding from the south of the Arabian peninsula to the Himalaya. Detailed investigations (not shown here) reveal that these anomalies only appear during boreal summer and we conclude that they result from a strengthening of the West African summer monsoon and a change in wind patterns (Kutzbach and Otto-Bliesner, 1982; Weldeab et al., 2007).

Saharan dust is transported across the Atlantic to the Amazon basin for $0k$, which agrees with simulated deposition patterns (Fig. 2). They are in agreement with patterns from other modeling studies for the pre-industrial era (Mahowald et al., 1999; Tegen et al., 2002).

3.1 Dust deposition rates in the North Atlantic: Comparison with marine sediment records

We verify our simulation results by comparing with data from marine sediment cores and sediment traps for the pre-industrial control (experiment $AO_{0k}LV_{0k}$; referred to as $0k$) and for the mid-Holocene (experiment $AO_{6k}LV_{6k}$; referred to as $6k$). An evaluation for both time slices is important because we are interested in differences in dust fluxes between $0k$ and $6k$.

Numerous studies of marine sediment records provide data of dust deposition rates in the North Atlantic Ocean which are comparable to our pre-industrial control simulation (see Table 4 and Fig. 3 for site locations). Only few studies present transient Holocene records of lithogenic dust fluxes in the Atlantic along the northwest African margin between 19°N and 31°N (deMenocal et al., 2000; Adkins et al., 2006; McGee et al., 2013; Albani et al., 2015). In those studies, the terrigenous fraction of the sediments was calculated by subtracting the carbonate, opal and organic carbon percentages from the total flux following Wefer and Fischer (1993). The studies of deMenocal et al. (2000) and Adkins et al. (2006) both investigate fluxes at core ODP Site 658C, but the latter study accounts for sediment redistribution via ^{230}Th normalization similar to McGee et al. (2013). Additionally, McGee et al. (2013) apply grain size endmember modeling to separate eolian and hemipelagic fluxes. Further, Albani et al. (2015) provides an updated observational dataset with higher temporal resolution and information about particle size distribution. All studies found large differences in dust accumulation between the mid-Holocene and the pre-industrial era.

We obtain simulated dust deposition rates in the grid cell whose midpoint is closest to the corresponding site location. The order of magnitude of the simulated fluxes is in agreement with data for both $0k$ and $6k$ (Fig. 4). Simulated pre-industrial dust deposition fluxes vary between 5.1 $gm^{-2}a^{-1}$ and 18.5 $gm^{-2}a^{-1}$ compared to an observed data range of 3.4 $gm^{-2}a^{-1}$ to 22 $gm^{-2}a^{-1}$. Simulated mid-Holocene deposition fluxes vary between 2.5 $gm^{-2}a^{-1}$ and 6 $gm^{-2}a^{-1}$ and thus slightly exceed those indicated by marine sediments (McGee et al., 2013), which range from 0.92 $gm^{-2}a^{-1}$ to 4.1 $gm^{-2}a^{-1}$ (Table 5). The spatial log correlation coefficient of observed and modeled values at different sites (Fig. 3) is 0.89 for $0k$ and 0.85 for $6k$. Changes in dust deposition between the mid-Holocene and pre-industrial era are depicted by calculating the ratio between the $0k$ and $6k$ simulated dust deposition rates corresponding to the sediment cores of McGee et al. (2013) and Adkins et al. (2006) (Table 5). The incremental factor of simulated dust deposition fluxes between $0k$ and $6k$ varies from 2.1 to 3.1 and increases monotonically from north to south. McGee et al. (2013) calculated a ratio between 3.7 and 5.4 between $0k$ and $6k$, whereas a ratio of 2.4 was found in the study of Adkins et al. (2006).

An increase of dust fluxes from north to south was observed by McGee et al. (2013). This is also seen in our model results (Fig. 5). To determine the north-south gradient, simulated dust deposition rates in the three ocean grid cells that are closest to the northwest African margin between 19°N and 27°N are considered (Fig. 5). We interpolate the simulated dust deposition fluxes linearly as a function of latitude applying the least square method (straight line in Fig. 5). For $0k$, simulated dust deposition rates increase thus by 1.76 $gm^{-2}a^{-1}$ per degree latitude; for $6k$, they increase by 0.67 $gm^{-2}a^{-1}$ per degree latitude. The north-south gradient obtained from marine sediment records (Table 4) differs slightly from ours with dust accumulation increasing by 2.55 $gm^{-2}a^{-1}$ per degree latitude for $0k$ and 1.47 $gm^{-2}a^{-1}$ per degree latitude for $6k$.

Additional to dust accumulation rates, McGee et al. (2013) and Albani et al. (2015) presented particle size distributions in the marine cores. Using end-member modeling, McGee et al. (2013) separated eolian inputs from hemipelagic inputs for $0k$ fluxes and presented best-fit Weibull functions to estimate the endmember contributions. We compare the size distribution of simulated deposition fluxes in the coarse mode (accounting for 98% of all aerosols) at the position of marine core GC68 to the observed dust size distribution in the sediment core as reported in Albani et al. (2015) for $0k$ and $6k$ and McGee et al. (2013) for $0k$ (Fig. 6). Marine core GC68 is representative for the cores GC49 and GC37, since simulations and observations show a similar distribution for those cores (not shown). Note that in our model output it was not possible to separate the size distribution of dust from the one of all aerosols. However, most other aerosols exist primarily in modes with a much smaller median diameter compared to dust. Dust is the only representative of the insoluble coarse mode. In the soluble coarse mode, only sea salt particles exist with an approximately similar mass mixing ratio as mineral dust. The concentration of the remaining aerosols is much lower in comparison. In our model output, we find a similar aerosol median diameter for soluble and insoluble

particles. Thus, we assume that the aerosol size distribution obtained from our model results is in principle representative for the dust size distribution.

We notice a quite similar particle distribution for $0k$ and $6k$ in our model results (Fig. 6). This is in agreement with observations and model results of Albani et al. (2015), who stated that during the Holocene the temporal variability of the dust size distribution is very limited. Compared to observations of Albani et al. (2015) and McGee et al. (2013), the simulated mean aerosol diameter is relatively small (Fig. 6). Mahowald et al. (2014) pointed out that the atmospheric surface concentrations are in general finer than the ones deposited in marine cores because coarser particles are removed preferentially from the atmosphere whereas finer particles are transported further downwind to the Atlantic Ocean. The particle size distribution of our study refers to dust deposition fluxes at the ocean's surface. We assume that they are still finer than the accumulated dust in the deep ocean. The mean diameter of our simulated size distribution of dust depostion fluxes is in average higher than the one of the modeled size distribution of atmospheric surface concentrations along the northwest African margin of Mahowald et al. (2014; Fig. 8k,l) but smaller than of observed values (Mahowald et al. 2014; Fig. 8k).

3.2 Influence of land surface conditions and atmosphere-ocean conditions on dust emission, transport and deposition

The simulated dust emission, atmospheric burden, total deposition and precipitation in North Africa (17°W - 40°E; 10°N - 30°N) and the global life time of dust in the atmosphere for the conducted experiments are summarized in Table 6. Additionally, percentages of wet deposition, dry deposition and sedimentation of the total deposition are presented. Standard deviations of the 30 year dust emission ensemble are given.

Pre-industrial land surface conditions result in much higher dust emission compared to mid-Holocene land surface conditions, independently of atmospheric and ocean boundary conditions. Emissions in North Africa are 3.3 to 3.8 times higher for AO_xLV_{0k} compared to AO_xLV_{6k} with $x \in \{0k, 6k\}$. Rates of deposition and the dust burden in the atmosphere in North Africa increase by a factor of 2.1 to 2.3 and 2.5 to 2.8, respectively. In experiment $AO_{6k}LV_{0k}$, the dust cycle is enhanced only slightly compared to the pre-industrial control ($AO_{0k}LV_{0k}$). On the other hand, for mid-Holocene land surface cover (LV_{6k}), mid-Holocene atmosphere-ocean conditions reduce emission and enhance deposition slightly (compare $AO_{0k}LV_{6k}$ and $AO_{6k}LV_{6k}$ in Table 6).

Is the suppression of dust emission by land surface conditions due to increased lake surface area or rather linked to enhanced vegetation cover? In experiments $AO_{6k}L_{0k}V_{6k}$ and $AO_{6k}L_{6k}V_{0k}$, we change lake surface area and vegetation cover separately; one is set to $6k$ conditions, while the other one remains in the pre-industrial state. In either experiment, dust emission is approximately halved and deposition reduces to about 70% compared to the pre-industrial control (Table 6). Emission and deposition fluxes are still higher than fluxes obtained with fully mid-Holocene land surface cover.

The burden is slightly higher for $AO_{6k}L_{6k}V_{0k}$ compared to $AO_{6k}L_{0k}V_{6k}$. In conclusion, paleolakes and mid-Holocene vegetation both contributed nearly to the same extent to a reduced dust cycle during the mid-Holocene.

About 20.6% of the simulated total deposition in North Africa is due to wet deposition for the pre-industrial control ($AO_{0k}LV_{0k}$) compared to about 51.1% for mid-Holocene conditions ($AO_{6k}LV_{6k}$) corresponding to increased annual rainfall from 0.66 mm day^{-1} to 1.97 mm day^{-1} (Table 6). Consequently, the global life time of dust in the atmosphere decreases from 4.4 to 3.7 days when mid-Holocene land surface is prescribed because particles are washed out more rapidly from the atmosphere. This result is almost unaffected by a change in orbit and ocean conditions. Only about 41% of Saharan dust is deposited in the emission area for pre-industrial conditions. Hence, a large amount of dust is transported downwind beyond North Africa to the North Atlantic and even reaching to the Amazon area (Fig. 2). In contrast, the ratio of deposited versus emitted dust in North Africa is about 75% for mid-Holocene conditions, which is related to shorter life times, enhanced rainfall and a higher impact of wet deposition.

3.3 Factor analysis of controls on dust emission and deposition

We separate the impacts of a) land surface conditions and b) atmosphere-ocean conditions on dust emission in North Africa and deposition fluxes in the North Atlantic along the northwest African margin applying the factor separation method of Stein and Alpert (1993) as briefly introduced in section 2.4. In Table 7, the total difference Δ_{6k-0k}, the contribution Δ_{AO} due to differences in orbital forcing, SST and SIC, the contribution Δ_{LV}, which captures the effects of changed land surface cover, and the synergy between both factors Δ_{SYN} are presented for dust emission in North Africa and deposition along the northwest African margin. Differences due to changes in land surface conditions Δ_{LV} differ not more than 5% from the total differences Δ_{6k-0k}. We conclude that land surface cover was the main control on dust emission in North Africa and associated deposition along the northwest African margin during the mid-Holocene. The impact of atmosphere-ocean conditions Δ_{AO} is even slightly negative for dust emission and has a negative effect of 16.5% of the total differences for dust deposition in the North Atlantic. The synergy effect accounts for 7.6% of dust emission and 20.4% of dust deposition.

Comparing patterns of dust emission in North Africa (Fig. 7) and dust deposition in the North Atlantic (Fig. 8) visually, emphasizes the high impact of land surface conditions. The patterns of the contribution Δ_{LV} and the total difference Δ_{6k-0k} are almost identical. Mid-Holocene atmosphere-ocean conditions with fixed pre-industrial land surface ($AO_{6k}L_{0k}$) lead to a change in dust emission only locally. Interestingly, we find an increase in dust emission from the Western Sahara, whereas less dust is emitted from the Bodélé Depression. Dust deposition in the North Atlantic does not differ significantly compared to the control and is even slightly enhanced between $10°$N and $15°$N. The

change in dust sources and deposition patterns is linked to a changed seasonal cycle (see Appendix A).

Relating Fig. 7 to Fig. 8, this analysis demonstrates that emission in North Africa is directly linked to deposition in the North Atlantic along the northwest African margin. In our simulations, we identify land surface conditions to be the main control on dust emission and deposition with a contribution of more than 95%. Changes in dust transport due to changes in atmospheric processes alone play a minor role.

4 Discussion and conclusion

We have explored whether the sudden increase in dust deposition fluxes in the North Atlantic Ocean between the mid-Holocene (6 ka BP) and pre-industrial era (1850 AD) as indicated by marine sediments (deMenocal et al., 2000; Adkins et al., 2006; McGee et al., 2013; Albani et al., 2015) were induced by variations in North African land surface cover or rather related to a change in atmosphere-ocean conditions. By simulating the dust cycle for both eras we have analyzed the relative contribution of those drivers to an enhanced dust cycle. In our simulations, orbital forcing parameters and ocean conditions are adjusted respectively and mid-Holocene land surface conditions are fixed according to vegetation reconstructions of Hoelzmann et al. (1998) and simulations of lake surface area (Tegen et al., 2002).

We find decreased dust activity in North Africa during the African Humid Period (AHP) at 6 ka BP, where dust emission fluxes from the Saharan desert are reduced to about 27% of pre-industrial fluxes and associated dust accumulation in the North Atlantic is reduced by a factor between 2.1 and 3.1 for specific site locations. The latter result is in agreement with a marine sediment record of Adkins et al. (2006) that indicates lower deposition fluxes by a factor of 2.4 for the mid-Holocene compared to pre-industrial, but not with the values of McGee et al. (2013), who find an average factor of 4.5 for those sites. McGee et al. (2013) argue that the amplitude of a change in dust flux is underestimated by Adkins et al. (2006) because the record does not separate eolian and fluvial/shelf inputs. The relatively low contrast of mid-Holocene and pre-industrial fluxes of our study compared to McGee et al. (2013) arise from higher mid-Holocene deposition rates in the North Atlantic, whereas pre-industrial fluxes are approximately similar. Despite the uncertainties in quantifying dust deposition fluxes, prescribing land surface cover according to paleorecords (Hoelzmann et al., 1998) reduces the deviation between simulated deposition and dust accumulation from marine records for the mid-Holocene compared to previous simulation studies (Albani et al., 2015). Comparing dust deposition fluxes at the surface to deep sea sediment accumulations while disregarding ocean currents and other disturbances could entail biases in the fluxes. However, Ratmeyer et al. (1999) argued that in the area of the chosen cores, there is a fast and mostly undisturbed downward transport of lithogenic material

in the water column. Thus, sedimentation fluxes mostly correlate well between upper and lower ocean depths and the surface.

We find a north-south increase of dust deposition rates along the northwest African margin during the mid-Holocene and pre-industrial era, which is consistent with observations of McGee et al. (2013). The increase in dust deposition with decreasing latitude can presumably be attributed to the wind climatology. According to the NCEP reanalysis (Kalnay et al., 1996), present day surface winds increase from north to south along the northwest African margin and can thus transport higher amounts of dust to the ocean. We compared the particle size distribution in the marine sediment cores presented by Albani et al. (2015) and McGee (2013) with the particle size distribution of simulated deposited aerosol fluxes. In agreement with observations (Albani et al., 2015), we find neither large spatial nor temporal variability in Holocene particle size distribution. Compared to observations of Albani et al. (2015) and McGee (2013), the simulated mean aerosol diameter is relatively small. We assume that dust deposition fluxes at the ocean's surface are in general finer than the accumulated dust in the deep ocean.

We identify land surface cover to be the main control on dust emission in North Africa and associated dust deposition in the North Atlantic. The direct link between patterns of dust emission fluxes in North Africa and deposition fluxes in the North Atlantic is demonstrated via a factor separation analysis. Enlarged lake surface area and expanded vegetation cover contribute equally to the reduced dust cycle of the mid-Holocene, although paleolakes covered a much smaller area than vegetation. Paleolakes suppressed dust emission completely on a particular area, whereas vegetation was spread out in the whole Sahara, but its type and distribution still enabled dust emission.

The vegetation at $6k$ consisted mainly of grasses and some shrubs and thus vegetation of low stature with a relatively low roughness length (compared to e.g. trees), which was somehow distributed in patches (Jolly et al., 1998). Thus, there still remained larger areas of bare soil, which served as sources of dust. In the model, a grid box is divided into fractions of bare soil and vegetation. Bare soil areas are potential dust sources. Additionally, (Stanelle et al., 2014) account for 'gaps' within the vegetated area, where dust emission can occur. Thus, although a relatively high vegetation fraction is prescribed for the mid-Holocene (58% for steppe and 80% for savanna), our model predicts a reasonable amount of emitted dust. Biases may occur from the rather simplistic reconstructed vegetation cover of (Hoelzmann et al., 1998) as homogenous vegetation is prescribed for a large area due to a lack of detailed information on vegetation cover. A more diverse vegetation cover could influence near surface winds. Dust emission occurs only above a threshold wind velocity and is very sensitive to changes in near surface winds. Hence, the distribution of vegetation surely influences dust emission locally. Nevertheless, we assume that the total amount of emitted dust and the corresponding deposited amount of dust in the North Atlantic is not significantly affected by a uniform vegetation distribution.

The prescribed mid-Holocene lake surface area rather represents the potential maximum areal lake extent obtained from filling up topographic depression assuming unlimited water supply (Tegen et al., 2002) resulting in a lake surface area of about 12% of North Africa, whereas paleoreconstructions assume a lake surface area of about 7.6% (Hoelzmann et al., 1998). Thus, dust emission is underestimated in our simulations due to suppression by lake coverage. Considering this bias, it seems likely that the relative importance of vegetation cover on the suppression of dust emission is higher than the one of lakes.

In addition to the direct suppression of mid-Holocene dust emission by extended land surface cover, land surface-precipitation feedbacks further reduced dust transport and deposition by changing wind and precipitation patterns (Coe and Bonan, 1997; Claussen et al., 1999; Rachmayani et al., 2015). In our simulations, those feedbacks are reflected by enhanced precipitation and a higher fraction of wet deposition compared to dry deposition and sedimentation during the mid-Holocene. Through enhanced precipitation dust particles are washed out more rapidly from the atmosphere. The fraction of wet deposition of the total deposition increases from about 20% at $0k$ to about 51% at $6k$ corresponding to a three times higher amount of rainfall and a decrease in global life time of dust. The partitioning of the direct masking effect by vegetation and lake surface cover and the indirect effect of land surface-climate feedbacks on a suppression of dust emission remains to be assessed. A change to mid-Holocene atmosphere-ocean conditions alone (experiment $AO_{6k}LV_{0k}$) affects the total amount of emitted and deposited dust only marginally compared to the control. They have, however, an impact on the seasonal dust cycle and dust source regions. In experiment $AO_{6k}LV_{0k}$, precipitation in the southern Sahara is enhanced by about 1 mm/day compared to 0k and the monsoon propagates further north during summer. Nevertheless, the amount of precipitation and the northward propagation of the West African monsoon during summer is underestimated in comparison with paleoevidence (Bartlein, 2011). This bias is common to most simulations of the PMIP intercomparison study (Braconnot et al., 2007). We found that in experiment $AO_{6k}LV_{6k}$, where additionally a more realistic land surface is prescribed for $6k$, precipitation is even overestimated in the southern Sahara and is in agreement with paleodata of Bartlein (2011) north of 20°N. Uncertainties in the simulated physical climate that arise from model biases for pre-industrial times are reported in Giorgetta et al. (2013) for MPI-ESM (including ECHAM6 as atmospheric general circulation model) in the frame of CMIP5. They mention a dry bias in the tropics over land north of the equator. However, since differences in precipitation between $6k$ and $0k$ are in agreement with paleoevidence, we assume the bias not to have a significant effect. A weakening of northeasterly winds in experiment $AO_{6k}LV_{6k}$ of about 3-4 m/s compared to the control run and of 2 m/s in experiment $AO_{6k}LV_{0k}$ was found during summer, which is related to the enhanced monsoon and precipitation. Weakened surface winds during winter are related to a reduction in coastal upwelling during the mid-Holocene as noted by Adkins et al. (2006) and Bradtmiller et al. (2016). In our simulations we do not find a substantial change in northeasterly winter winds during the Holocene which might be due to a

general underestimation of high-speed wind events by the relatively coarse global-scale GCMs (e.g. Capps and Zender (2008)).

The implications of an abrupt increase in dust deposition on the characterization of the Holocene landscape transformation remains to be assessed. Do land surface-climate feedbacks generate a sudden reduction of vegetation cover or lake surface area, resulting in a sudden exposure of dust source areas? Or can the abrupt change in dust deposition in the North Atlantic be interpreted as a non-linear response of Saharan dust emission to a steadily changing surface? Do multiple equilibria or bifurcations emerge from the interaction of dust, vegetation and climate? These questions will have to be addressed by transient climate simulations including interactive vegetation and a scheme that dynamically simulates the extent of surface water areas following Stacke and Hagemann (2012) into the climate-aerosol model.

Acknowledgement. We thank Stefan Hagemann for review, Andrea Kay for spelling correction and acknowledge the valuable input of four anonymous reviewers. The ECHAM-HAMMOZ model is developed by a consortium composed of ETH Zurich, Max Planck Institut für Meteorologie, Forschungszentrum Jülich, University of Oxford, the Finnish Meteorological Institute and the Leibniz Institute for Tropospheric Research, and is managed by the Center for Climate Systems Modeling (C2SM) at ETH Zurich. The service charges for this open-access publication have been covered by the Max Planck Society.

References

Adkins, J., deMenocal, P., and Eshel, G.: The "African Humid Period" and the Record of Marine Upwelling from Excess 230Th in ODP Hole 658C, Paleoceanography, 21, doi:doi:10.1029/2005PA001200, 2006.

Albani, S., Mahowald, N. M., Winckler, G., Anderson, R. F., Bradtmiller, L. I., Delmonte, B., François, R., Goman, M., Heavens, N. G., Hesse, P. P., Hovan, S. A., Kang, S. G., Kohfeld, K. E., Lu, H., Maggi, V., Mason, J. A., Mayewski, P. A., McGee, D., Miao, X., Otto-Bliesner, B. L., Perry, A. T., Pourmand, A., Roberts, H. M., Rosenbloom, N., Stevens, T., and Sun, J.: Twelve thousand years of dust: the Holocene global dust cycle constrained by natural archives, Climate of the Past, 11, 869–903, doi:10.5194/cp-11-869-2015, http://www.clim-past.net/11/869/2015/, 2015.

Armitage, S. J., Bristow, C. S., and Drake, N. A.: West African monsoon dynamics inferred from abrupt fluctuations of Lake Mega-Chad, Proceedings of the National Academy of Sciences, doi:10.1073/pnas.1417655112, 2015.

Bartlein, P.: Pollen-based continental climate reconstructions at 6 and 21 ka: a global synthesis, Climate Dynamics, 37, 775–802, doi:10.1007/s00382-010-0904-1, 2011.

Berger, A.: Long-term variations of daily insolation and quaternary climatic changes, J. Atmos. Sci., 35, 2362–2367, 1978.

Bory, A. J.-M. and Newton, P. P.: Transport of airborne lithogenic material down through the water column in two contrasting regions of the eastern subtropical North Atlantic Ocean, Global Biogeochemical Cycles, 14, 297–315, doi:10.1029/1999GB900098, 2000.

Braconnot, P., Otto-Bliesner, B., Harrison, S., Joussaume, S., Peterchmitt, J.-Y., Abe-Ouchi, A., Crucifix, M., Driesschaert, E., Fichefet, T., Hewitt, C. D., Kageyama, M., Kitoh, A., Laîné, A., Loutre, M.-F., Marti, O., Merkel, U., Ramstein, G., Valdes, P., Weber, S. L., Yu, Y., and Zhao, Y.: Results of PMIP2 coupled simulations of the Mid-Holocene and Last Glacial Maximum – Part 1: experiments and large-scale features, Climate of the Past, 3, 261–277, doi:10.5194/cp-3-261-2007, http://www.clim-past.net/3/261/2007/, 2007.

Bradtmiller, L. I., McGee, D., Awalt, M., Evers, J., Yerxa, H., Kinsley, C. W., and deMenocal deMenocal deMenocal deMenocal deMenocal deMenocal deMenocal, P. B.: Changes in biological productivity along the northwest African margin over the past 20,000 years, Paleoceanography, 31, 185–202, doi:10.1002/2015PA002862, http://dx.doi.org/10.1002/2015PA002862, 2015PA002862, 2016.

Brovkin, V., Claussen, M., Petoukhov, V., and Ganopolski, A.: On the stability of the atmosphere-vegetation system in the Sahara/Sahel region, Journal of Geophysical Research: Atmospheres, 103, 31 613–31 624, doi:10.1029/1998JD200006, 1998.

Capps, S. B. and Zender, C. S.: Observed and CAM3 GCM Sea Surface Wind Speed Distributions: Characterization, Comparison, and Bias Reduction., Journal of Climate, 21, 6569–6585, doi:doi:10.1175/2008JCLI2374.1, 2008.

Carlson, T. and Prospero, J.: The large-scale movement of Saharan Air outbreaks over the Northern Equatorial Atlantic, J. Appl. Meteor., 11, 283–297, 1972.

Claussen, M., Kubatzki, C., Brovkin, V., Ganopolski, A., Hoelzmann, P., and Pachur, H.-J.: Simulation of an abrupt change in Saharan vegetation in the Mid-Holocene, Geophysical Research Letters, 26, 2037–2040, doi:10.1029/1999GL900494, 1999.

Cockerton, H. E., Holmes, J. A., Street-Perrott, F. A., and Ficken, K. J.: Holocene dust records from the West African Sahel and their implications for changes in climate and land surface conditions, Journal of Geophysical Research: Atmospheres, 119, 8684–8694, doi:10.1002/2013JD021283, 2014.

Coe, M. T. and Bonan, G. B.: Feedbacks between climate and surface water in northern Africa during the middle Holocene, Journal of Geophysical Research: Atmospheres, 102, 11 087–11 101, doi:10.1029/97JD00343, http://dx.doi.org/10.1029/97JD00343, 1997.

deMenocal, P., Ortiz, J., Guilderson, T., Adkins, J., Sarnthein, M., Baker, L., and Yarusinsky, M.: Abrupt onset and termination of the African Humid Period:: rapid climate responses to gradual insolation forcing, Quaternary Science Reviews, 19, 347–361, 2000.

Doherty, R., Kutzbach, J., Foley, J., and Pollard, D.: Fully coupled climate/dynamical vegetation model simulations over Northern Africa during the mid-Holocene, Climate Dynamics, 16, 561–573, doi:10.1007/s003820000065, 2000.

Engelstaedter, S. and Washington, R.: Atmospheric controls on the annual cycle of North African dust, Journal of Geophysical Research: Atmospheres, 112, doi:10.1029/2006JD007195, http://dx.doi.org/10.1029/2006JD007195, 2007.

Fischer, G., Donner, B., Ratmeyer, V., Davenport, R., and Wefer, G.: Distinct year-to-year flux variations off Cape Blanc during 1988-1991: relation to 18O-deduced sea-surface temperatures and trade winds, Journal of Marine Research, 54, 73–98, 1996.

Gasse, F.: Hydrological changes in the African tropics since the Last Glacial Maximum, Quaternary Science Reviews, 19, 189–211, doi:http://dx.doi.org/10.1016/S0277-3791(99)00061-X, http://www.sciencedirect.com/science/article/pii/S027737919900061X, 2000.

Giorgetta, M. A., Jungclaus, J., Reick, C. H., Legutke, S., Bader, J., Böttinger, M., Brovkin, V., Crueger, T., Esch, M., Fieg, K., Glushak, K., Gayler, V., Haak, H., Hollweg, H.-D., Ilyina, T., Kinne, S., Kornblueh, L., Matei, D., Mauritsen, T., Mikolajewicz, U., Mueller, W., Notz, D., Pithan, F., Raddatz, T., Rast, S., Redler, R., Roeckner, E., Schmidt, H., Schnur, R., Segschneider, J., Six, K. D., Stockhause, M., Timmreck, C., Wegner, J., Widmann, H., Wieners, K.-H., Claussen, M., Marotzke, J., and Stevens, B.: Climate and carbon cycle changes from 1850 to 2100 in MPI-ESM simulations for the Coupled Model Intercomparison Project phase 5, Journal of Advances in Modeling Earth Systems, 5, 572–597, doi:10.1002/jame.20038, http://dx.doi.org/10.1002/jame.20038, 2013.

Hagemann, S.: An improved land surface parameter dataset for global and regional climate models, MPI Report No. 289, Max Planck Institute for Meteorology, Hamburg, 2002.

Harrison, S. P., Kohfeld, K. E., Roelandt, C., and Claquin, T.: The role of dust in climate changes today, at the last glacial maximum and in the future, Earth-Science Reviews, 54, 43–80, doi:http://dx.doi.org/10.1016/S0012-8252(01)00041-1, http://www.sciencedirect.com/science/article/pii/S0012825201000411, recent research on loess and palaeosols, pure and applied, 2001.

Hoelzmann, P., Jolly, D., Harrison, S. P., Laarif, F., Bonnefille, R., and Pachur, H.-J.: Mid-Holocene land-surface conditions in northern Africa and the Arabian Peninsula: A data set for the analysis of biogeophysical feedbacks in the climate system, Global Biogeochemical Cycles, 12, 35–51, doi:10.1029/97GB02733, http://dx.doi.org/10.1029/97GB02733, 1998.

Huneeus, N., Schulz, M., Balkanski, Y., Griesfeller, J., Prospero, J., Kinne, S., Bauer, S., Boucher, O., Chin, M., Dentener, F., Diehl, T., Easter, R., Fillmore, D., Ghan, S., Ginoux, P., Grini, A., Horowitz, L., Koch, D., Krol, M. C., Landing, W., Liu, X., Mahowald, N., Miller, R., Morcrette, J.-J., Myhre, G., Penner, J., Perlwitz, J., Stier, P., Takemura, T., and Zender, C. S.: Global dust model intercomparison in AeroCom phase I, Atmospheric Chemistry and Physics, 11, 7781–7816, doi:10.5194/acp-11-7781-2011, http://www.atmos-chem-phys.net/11/7781/2011/, 2011.

Irizarry-Ortiz, M. M., Wang, G., and Eltahir, E. A. B.: Role of the biosphere in the mid-Holocene climate of West Africa, Journal of Geophysical Research: Atmospheres, 108, ACL 5–1–ACL 5–15, doi:10.1029/2001JD000989, http://dx.doi.org/10.1029/2001JD000989, 4042, 2003.

Jickells, T., Newton, P., King, P., Lampitt, R., and Boutle, C.: A comparison of sediment trap records of particle fluxes from 19 to 48°N in the northeast Atlantic and their relation to surface water productivity, Deep Sea Research Part I: Oceanographic Research Papers, 43, 971–986, doi:http://dx.doi.org/10.1016/0967-0637(96)00063-5, http://www.sciencedirect.com/science/article/pii/0967063796000635, 1996.

Jolly, D., Prentice, I. C., Bonnefille, R., Ballouche, A., Bengo, M., Brenac, P., Buchet, G., Burney, D., Cazet, J.-P., Cheddadi, R., Edorh, T., Elenga, H., Elmoutaki, S., Guiot, J., Laarif, F., Lamb, H., Lezine, A.-M., Maley, J., Mbenza, M., Peyron, O., Reille, M., Reynaud-Farrera, I., Riollet, G., Ritchie, J. C., Roche, E., Scott, L., Ssemmanda, I., Straka, H., Umer, M., Van Campo, E., Vilimumbalo, S., Vincens, A., and Waller, M.: Biome reconstruction from pollen and plant macrofossil data for Africa and the Arabian peninsula at 0 and 6000 years, Journal of Biogeography, 25, 1007–1027, doi:10.1046/j.1365-2699.1998.00238.x, http://dx.doi.org/10.1046/j.1365-2699.1998.00238.x, 1998.

Kalnay, E., Kanamitsu, M., Kistler, R., Collins, W., Deaven, D., Gandin, L., Iredell, M., Saha, S., White, G., Woollen, J., Zhu, Y., Leetmaa, A., Reynolds, R., Chelliah, M., Ebisuzaki, W., Higgins, W., Janowiak, J., Mo, K. C., Ropelewski, C., Wang, J., Jenne, R., and Joseph, D.: The NCEP/NCAR 40-Year Reanalysis Project, Bulletin of the American Meteorological Society, 77, 437–471, 1996.

Kohfeld, K. and Harrison, S.: How well can we simulate past climates? Evaluating the models using global palaeoenvironmental datasets, Quaternary Science Reviews, 19, 321–346, doi:http://dx.doi.org/10.1016/S0277-3791(99)00068-2, http://www.sciencedirect.com/science/article/pii/S0277379199000682, 2000.

Kremling, K. and Streu, P.: Saharan dust influenced trace element fluxes in deep North Atlantic subtropical waters, Deep Sea Research Part I: Oceanographic Research Papers, 40, 1155–1168, doi:http://dx.doi.org/10.1016/0967-0637(93)90131-L, http://www.sciencedirect.com/science/article/pii/096706379390131L, 1993.

Kröpelin, S., Verschuren, D., Lézine, A.-M., Eggermont, H., Cocquyt, C., Francus, P., Cazet, J.-P., Fagot, M., Rumes, B., Russell, J. M., Darius, F., Conley, D. J., Schuster, M., von Suchodoletz, H., and Engstrom, D. R.: Climate-Driven Ecosystem Succession in the Sahara: The Past 6000 Years, Science, 320, 765–768, doi:10.1126/science.1154913, http://www.sciencemag.org/content/320/5877/765.abstract, 2008.

Kutzbach, J. E.: Monsoon Climate of the Early Holocene: Climate Experiment with the Earth's Orbital Parameters for 9000 Years Ago, Science, 214, 59–61, doi:10.1126/science.214.4516.59, http://www.sciencemag.org/content/214/4516/59.abstract, 1981.

Kutzbach, J. E. and Otto-Bliesner, B. L.: The sensitivity of the african-asian monsoonal climate to orbital parameter changes for 9000 years b.p. in a low-resolution general circulation model., J. Atmos. Sci., 39, 1177–1188, 1982.

Kutzbach, J. E. and Street-Perrott, F. A.: Milankovitch forcing of fluctuations in the level of tropical lakes from 18 to 0 kyr BP, Nature, 317, 130–134, 1985.

Mahowald, N., Kohfeld, K., Hansson, M., Balkanski, Y., Harrison, S. P., Prentice, I. C., Schulz, M., and Rodhe, H.: Dust sources and deposition during the last glacial maximum and current climate: A comparison of model results with paleodata from ice cores and marine sediments, Journal of Geophysical Research: Atmospheres, 104, 15 895–15 916, doi:10.1029/1999JD900084, http://dx.doi.org/10.1029/1999JD900084, 1999.

Mahowald, N., Albani, S., Kok, J. F., Engelstaeder, S., Scanza, R., Ward, D. S., and Flanner, M. G.: The size distribution of desert dust aerosols and its impact on the Earth system, Aeolian Research, 15, 53–71, doi:http://dx.doi.org/10.1016/j.aeolia.2013.09.002, http://www.sciencedirect.com/science/article/pii/S1875963713000736, 2014.

Marticorena, B. and Bergametti, G.: Modeling the atmospheric dust cycle: 1. Design of a soil-derived dust emission scheme, Journal of Geophysical Research: Atmospheres, 100, 16 415–16 430, doi:10.1029/95JD00690, http://dx.doi.org/10.1029/95JD00690, 1995.

Marticorena, B., Bergametti, G., Aumont, B., Callot, Y., N'Doumé, C., and Legrand, M.: Modeling the atmospheric dust cycle: 2. Simulation of Saharan dust sources, Journal of Geophysical Research: Atmospheres, 102, 4387–4404, doi:10.1029/96JD02964, http://dx.doi.org/10.1029/96JD02964, 1997.

McGee, D.: Reconstructions of eolian dust accumulation in northwest African margin sediments., doi:doi:10.1594/PANGAEA.836112, 2013.

McGee, D., deMenocal, P., Winckler, G., Stuut, J., and Bradtmiller, L.: The magnitude, timing and abruptness of changes in North African dust deposition over the last 20,000 yr, Earth and Planetary Science Letters, 371–372, 163–176, doi:http://dx.doi.org/10.1016/j.epsl.2013.03.054, http://www.sciencedirect.com/science/article/pii/S0012821X13001817, 2013.

Middleton, N. J. and Goudie, A. S.: Saharan dust: sources and trajectories, Transactions of the Institute of British Geographers, 26, 165–181, doi:10.1111/1475-5661.00013, http://dx.doi.org/10.1111/1475-5661.00013, 2001.

Perez-Sanz, A., Li, G., González-Sampériz, P., and Harrison, S. P.: Evaluation of modern and mid-Holocene seasonal precipitation of the Mediterranean and northern Africa in the CMIP5 simulations, Climate of the Past, 10, 551–568, doi:10.5194/cp-10-551-2014, http://www.clim-past.net/10/551/2014/, 2014.

Prentice, I. C., Jolly, D., and 6000 Participants, B.: Mid-Holocene and Glacial-Maximum Vegetation Geography of the Northern Continents and Africa, Journal of Biogeography, 27, pp. 507–519, http://www.jstor.org/stable/2656208, 2000.

Rachmayani, R., Prange, M., and Schulz, M.: North African vegetation–precipitation feedback in early and mid-Holocene climate simulations with CCSM3-DGVM, Climate of the Past, 11, 175–185, doi:10.5194/cp-11-175-2015, http://www.clim-past.net/11/175/2015/, 2015.

Ratmeyer, V., Fischer, G., and Wefer, G.: Lithogenic particle fluxes and grain size distributions in the deep ocean off northwest Africa: Implications for seasonal changes of aeolian dust input and downward transport, Deep

Sea Research Part I: Oceanographic Research Papers, 46, 1289–1337, doi:http://dx.doi.org/10.1016/S0967-0637(99)00008-4, http://www.sciencedirect.com/science/article/pii/S0967063799000084, 1999.

Schuster, M., Roquin, C., Duringer, P., Brunet, M., Caugy, M., Fontugne, M., Mackaye, H. T., Vignaud, P., and Ghienne, J.-F.: Holocene Lake Mega-Chad palaeoshorelines from space, Quaternary Science Reviews, 24, 1821–1827, doi:http://dx.doi.org/10.1016/j.quascirev.2005.02.001, http://www.sciencedirect.com/science/article/pii/S0277379105000831, 2005.

Stacke, T. and Hagemann, S.: Development and evaluation of a global dynamical wetlands extent scheme, Hydrology and Earth System Sciences, 16, 2915–2933, doi:10.5194/hess-16-2915-2012, 2012.

Stanelle, T., Bey, I., Raddatz, T., Reick, C., and Tegen, I.: Anthropogenically induced changes in twentieth century mineral dust burden and the associated impact on radiative forcing, Journal of Geophysical Research: Atmospheres, 119, 13,526–13,546, doi:10.1002/2014JD022062, http://dx.doi.org/10.1002/2014JD022062, 2014.

Stein, U. and Alpert, P.: Factor separation in numerical simulations, J. Atmos. Sci., 50, 2107–2115, 1993.

Stier, P., Feichter, J., Kinne, S., Kloster, S., Vignati, E., Wilson, J., Ganzeveld, L., Tegen, I., Werner, M., Balkanski, Y., Schulz, M., Boucher, O., Minikin, A., and Petzold, A.: The aerosol-climate model ECHAM5-HAM, Atmospheric Chemistry and Physics, 5, 1125–1156, doi:10.5194/acp-5-1125-2005, http://www.atmos-chem-phys.net/5/1125/2005/, 2005.

Street-Perrott, F., Marchand, D., Roberts, N., and Harrison, S. O. U. U. G. S.: Global lake-level variations from 18,000 to 0 years ago: A palaeoclimate analysis, 1989.

Sudarchikova, N.: Modeling of mineral dust in the Southern Hemisphere with focus on Antarctica for interglacial and glacial climate conditions, Ph.D. thesis, Universität Hamburg, 2012.

Sudarchikova, N., Mikolajewicz, U., Timmreck, C., O'Donnell, D., Schurgers, G., Sein, D., and Zhang, K.: Modelling of mineral dust for interglacial and glacial climate conditions with a focus on Antarctica, Climate of the Past, 11, 765–779, doi:10.5194/cp-11-765-2015, http://www.clim-past.net/11/765/2015/, 2015.

Taylor, K. E., Stouffer, R., and Meehl, G.: An overview of CMIP5 and the experiment design, Bull. Amer. Meteorol. Soc., 93, 485–498, 2011.

Tegen, I., Harrison, S. P., Kohfeld, K., Prentice, I. C., Coe, M., and Heimann, M.: Impact of vegetation and preferential source areas on global dust aerosol: Results from a model study, Journal of Geophysical Research: Atmospheres, 107, AAC 14–1–AAC 14–27, doi:10.1029/2001JD000963, http://dx.doi.org/10.1029/2001JD000963, 2002.

Tiedemann, R., Sarnthein, M., and Stein, R.: Climatic changes in the western Sahara: Aeolo-marine sediment record of the last 8 million years (Sites 657-661), Proceedings ODP, Scientific results, 108, 241–278, 1989.

Wefer, G. and Fischer, G.: Seasonal patterns of vertical particle flux in equatorial and coastal upwelling areas of the eastern Atlantic, Deep Sea Research Part I: Oceanographic Research Papers, 40, 1613–1645, doi:http://dx.doi.org/10.1016/0967-0637(93)90019-Y, http://www.sciencedirect.com/science/article/pii/096706379390019Y, 1993.

Weldeab, S., Lea, D. W., Schneider, R. R., and Andersen, N.: 155,000 Years of West African Monsoon and Ocean Thermal Evolution, Science, 316, 1303–1307, doi:10.1126/science.1140461, http://www.sciencemag.org/content/316/5829/1303.abstract, 2007.

Zhang, K., O'Donnell, D., Kazil, J., Stier, P., Kinne, S., Lohmann, U., Ferrachat, S., Croft, B., Quaas, J., Wan, H., Rast, S., and Feichter, J.: The global aerosol-climate model ECHAM-HAM, version 2: sensitivity to improvements in process representations, Atmospheric Chemistry and Physics, 12, 8911–8949, doi:10.5194/acp-12-8911-2012, http://www.atmos-chem-phys.net/12/8911/2012/, 2012.

Appendix A

Wind patterns and annual cycle

An analysis of the seasonal cycle of dust emission in relation to meteorological conditions is provided to get a deeper understanding of our simulation results. We present the seasonal cycle of dust emission for our main experiments and relate them to seasonal wind patterns.

North African dust emission is linked to a distinct seasonal cycle (Engelstaedter and Washington, 2007). Northeasterly near surface trade winds below 1000m height are responsible for the majority of dust transport from the Saharan desert toward the North Atlantic during the winter months (Ratmeyer et al., 1999; Engelstaedter and Washington, 2007). In our simulations, northeasterly winds are strongest along the coast during winter (Fig. 9, top). Accordingly, maximum dust emission rates occur from January till April (Fig. 10). Dust production in the Western Sahara becomes active towards the summer. Dust is then lifted up and transported by the Harmattan or Saharan Air Layer (SAL) (Carlson and Prospero, 1972), that is coupled to the African Easterly Jet at 1000m to 5000m height (Tiedemann et al., 1989). Accordingly, the convergence belt is shifted northwards during boreal summer. We notice a second smaller peak of dust emission around June in the control run. Dust activity decreases by the end of the year in all regions (Fig. 10). The Bodélé Depression in central Chad is active throughout most of the year. In this region, dust is emitted and lifted up by Harmattan winds.

Mid-Holocene wind patterns hardly change during winter compared to the pre-industrial control, whereas during the summer months the ITCZ propagates further north (Fig. 9, middle). Wind fields from the Eastern Atlantic Ocean to the Sahel area in the southwest induced by the West African monsoon extent further north. Consequently, the transport of dust from North Africa to the North Atlantic is reduced.

If orbital forcing is adjusted to mid-Holocene conditions and pre-industrial land surface is kept ($AO_{6k}LV_{0k}$), we obtain only a slight increase in annual dust emission (section 3.2) in our simulations, but the seasonal cycle changes significantly (Fig. 10, bottom left). The corresponding patterns of simulated dust emission show an enhanced dust productivity in the Western Sahara compared to the control run (section 3.3), where dust productivity increases toward the summer (Engelstaedter and Washington, 2007). Accordingly, dust emission is highest during summer in our simulation (June to August). Although the total amount of annual dust emission hardly changes, there is a clear shift in source regions and the seasonal cycle when only mid-Holocene atmosphere-ocean conditions are set. Dust emission is strongly prevented throughout the year when mid-Holocene vegetation and lakes are prescribed (LV_{6k}). Hereby, the seasonal cycle of dust emission is closely linked to the seasonal plant growth. The leaf area index and the soil moisture increase during the summer months, when the West African monsoon becomes active. Nonetheless, the change of atmosphere-ocean conditions from $0k$ to $6k$ tends to shift the time of maximal dust productivity from March-May to May-July (compare $AO_{0k}LV_{6k}$ and $AO_{6k}LV_{6k}$).

The analysis of the seasonal cycle of dust emission shows that mid-Holocene land surface cover suppresses dust emission throughout the year, which results in reduced annual dust emission. Although mid-Holocene atmosphere-ocean conditions do not provoke a significant change of the total annual amount of emitted dust in North Africa, they affect the atmospheric circulation, what is reflected in a changed seasonal cycle and a shift of dust source regions.

Appendix B

Precipitation and wind changes

We explicitly investigate changes in simulated wind and precipitation between experiment $AO_{6k}LV_{0k}$ and $AO_{6k}LV_{6k}$ and the control run, respectively, and compare to paleoevidence (Bartlein, 2011) to ensure that Holocene climate variability is not underestimated by our model.

Precipitation is enhanced up to 1 mm/day in the $AO_{6k}LV_{0k}$ simulation compared to the control run (Fig. 11), which is consistent with the PMIP results Braconnot et al. (2007). In general, global circulation models (GCM) underestimate the extent of the North African summer monsoon and precipitation during the mid-Holocene (Braconnot et al., 2007; Perez-Sanz et al., 2014). Thus, several studies emphasize the role of land cover-precipitation feedbacks to be crucial when simulating mid-Holocene climate in North Africa (Claussen et al., 1999; Irizarry-Ortiz et al., 2003; Rachmayani et al., 2015).

In experiment $AO_{6k}LV_{6k}$, the increase in precipitation compared to the pre-industrial control is up to 4 mm/day in the southern Sahara due to enhanced vegetation and lake surface area and related feedbacks. Between 10°N and 20°N the model overestimates the increase in precipitation compared to paleoevidence (Bartlein, 2011), but north of 20°N an increase of 1-2 mm/day in North Africa seems realistic. In conclusion, enhanced vegetation cover and lake surface area do not only have a direct effect by covering source areas and hence suppressing dust emission, but additionally land surface-precipitation feedbacks cause enhanced washing out of particles by rainfall.

We notice a weakening of northeasterly winds of about 3-4 m/s during the summer in experiment $AO_{6k}LV_{6k}$ compared to the control (Fig. 9, middle), whereas northeasterly winds decrease about 2 m/s in experiment $AO_{6k}LV_{0k}$. Changes in wind patterns are most likely related to a northward shift of the monsoon and enhanced precipitation during the summer. Thus, we ensure that wind changes are not underestimated by the model, because in contrast to most GCM, the increase in precipitation is not underestimated in experiment $AO_{6k}LV_{6k}$, when prescribing a more realistic mid-Holocene land surface cover. Northeasterly winter winds do not change very much, neither for experiment $AO_{6k}LV_{6k}$ nor for experiment $AO_{6k}LV_{6k}$. This is in contrast to Bradtmiller et al. (2016), who suggest a significant decrease in winter surface winds as the cause of a reduction in coastal upwelling and productivity. This may be related to a general underestimation of high-speed wind events in GCMs (e.g. Capps and Zender (2008)).

List of Figures

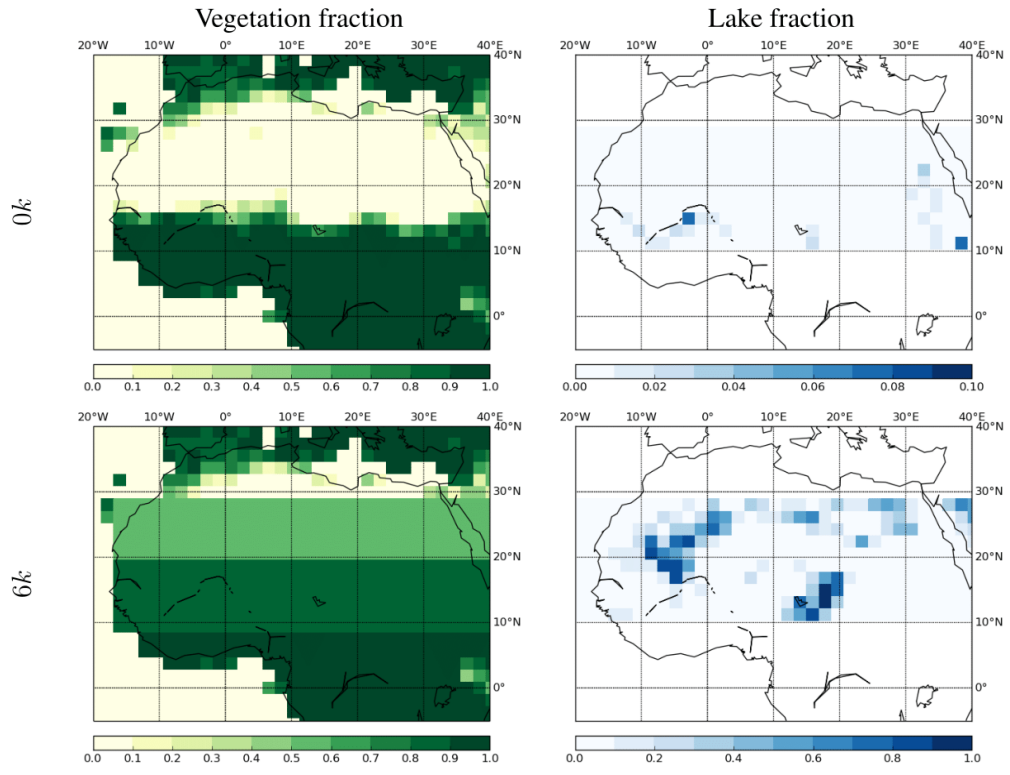

Figure 1. Vegetation and lake fraction for $0k$ and $6k$. $6k$ lake fraction is obtained from Tegen et al. (2002) and $6k$ vegetation fraction is reconstructed following Hoelzmann et al. (1998). Note that lake fraction is scaled differently for $0k$ and $6k$.

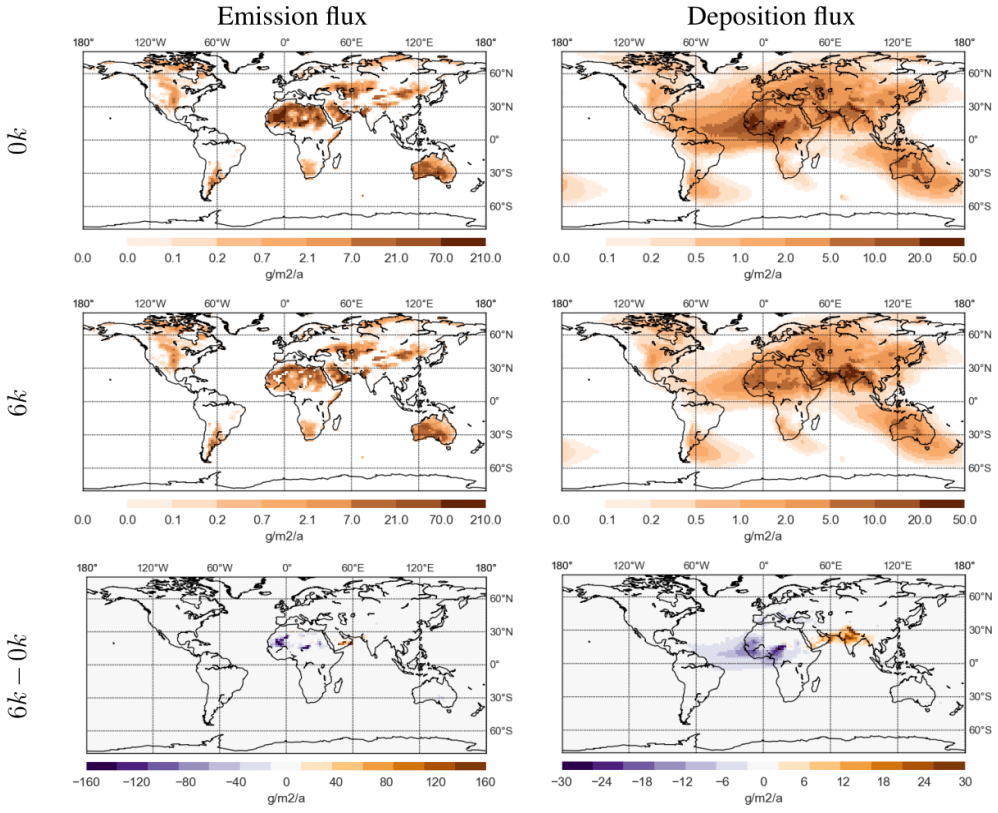

Figure 2. Simulated global annual mean dust emission flux (left) and dust deposition flux (right) for $0k$, $6k$ and for the difference $6k$-$0k$.

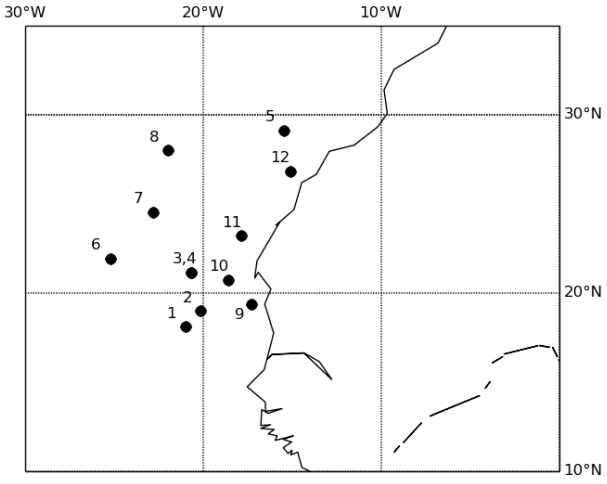

Figure 3. Site locations of marine sediment cores and sediment traps along the northwest African margin corresponding to Table 4.

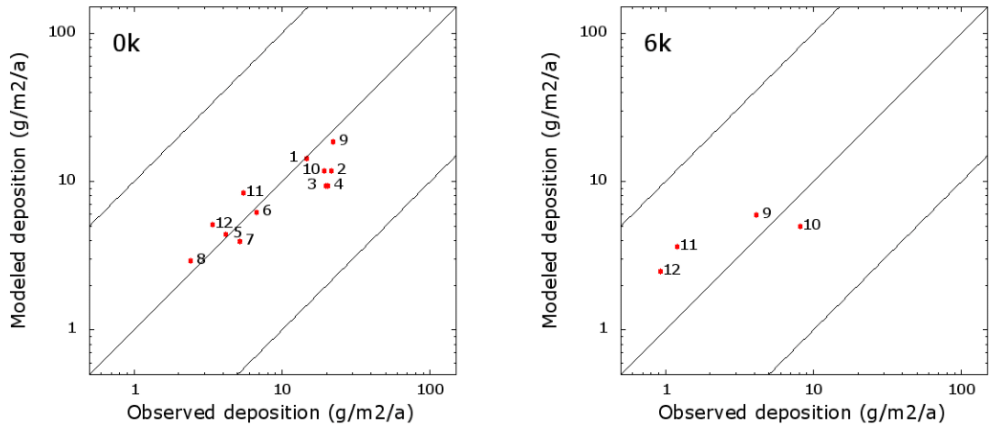

Figure 4. Simulated dust deposition flux for $0k$ (left, $AO_{0k}LV_{0k}$) and $6k$ (right, $AO_{6k}LV_{6k}$) compared with data from marine sediment cores and sediment traps (Table 4). Log correlation coefficients are: 0.89 ($0k$) and 0.85 ($6k$).

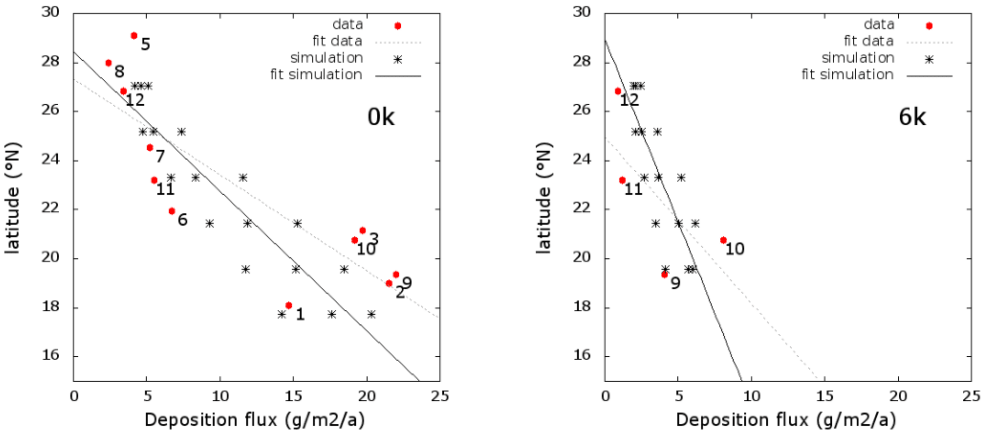

Figure 5. Simulated dust deposition flux for the three ocean grid cells that are closest to the northwest African margin for $0k$ (left) and $6k$ (right) at different latitudes compared with data from marine sediment cores and sediment traps (Table 4). The straight lines are linear interpolations obtained with the least square method.

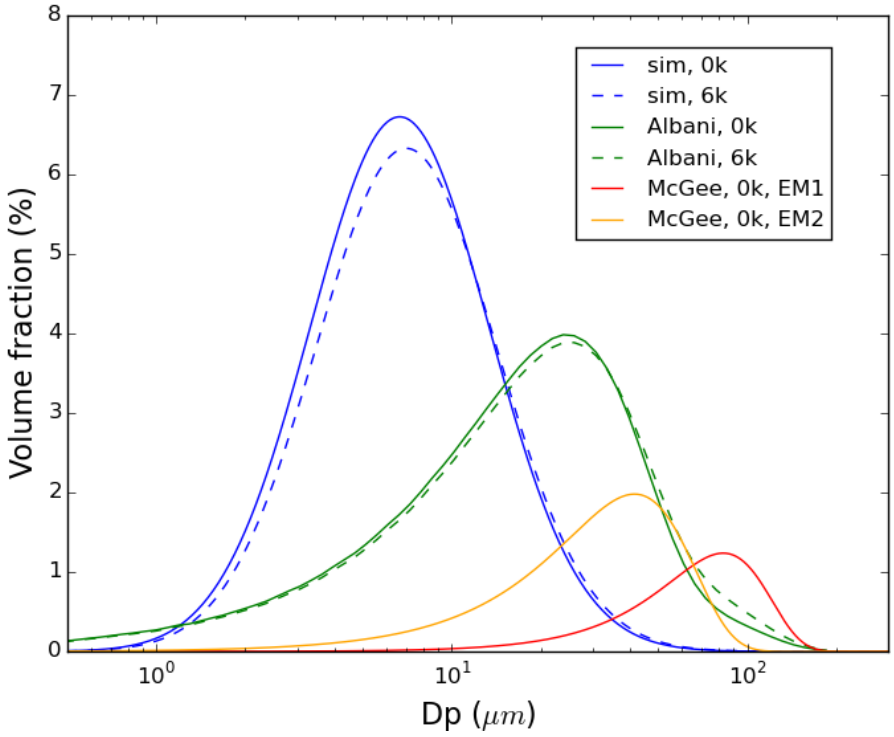

Figure 6. Simulated aerosol size distribution of deposited fluxes at the position of marine core GC68 (blue), dust size distribution in the sediment core of Albani et al. (2015) (green) for $0k$ (solid) and $6k$ (dotted) and best-fit Weibull functions that represent the contribution of the endmember corresponding to eolian inputs (endmember 1 (EM1, red) and 2 (EM2, orange) in McGee (2013)) for $0k$. Curves are normalized to an area of 1.

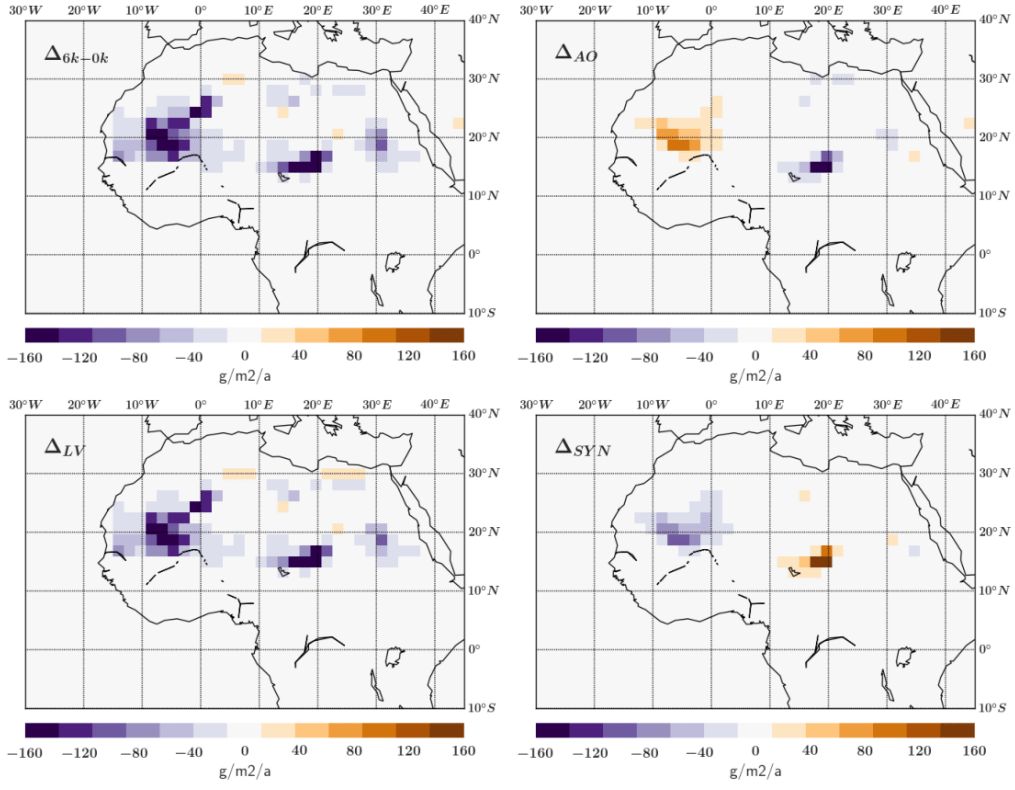

Figure 7. Differences in simulated dust emission in North Africa (17°W - 40°E; 10°N - 30°N) between $6k$ and $0k$, Δ_{6k-0k} (top left), Δ_{AO} (top right), Δ_{LV} (bottom left) and the synergy effect Δ_{SYN} (bottom right).

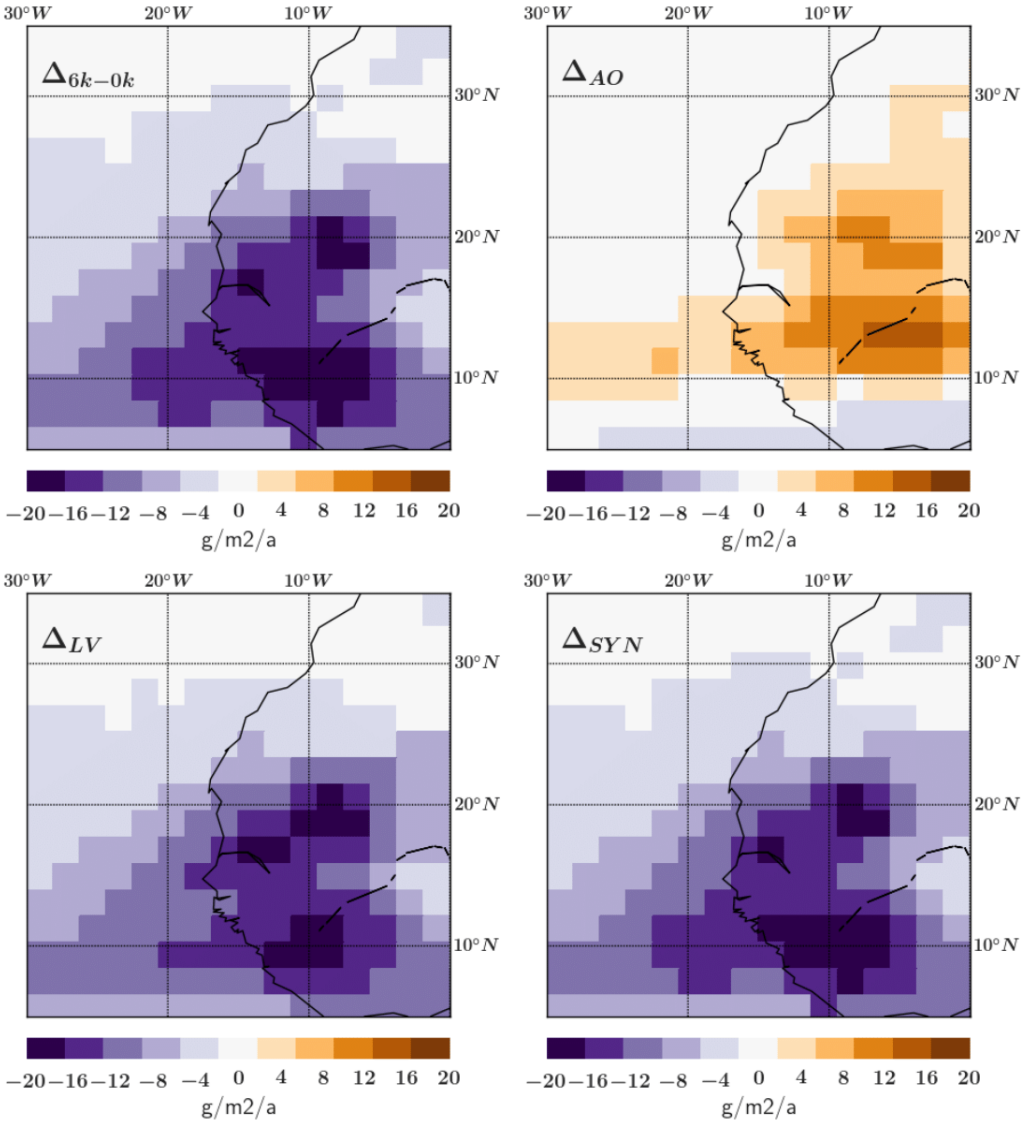

Figure 8. Differences in simulated dust deposition along the northwest African margin (30°W - 17°W; 5°N - 35°N) between $6k$ and $0k$ Δ_{6k-0k} (top left), Δ_{AO} (top right), Δ_{LV} (bottom left) and the synergy effect Δ_{SYN} (bottom right).

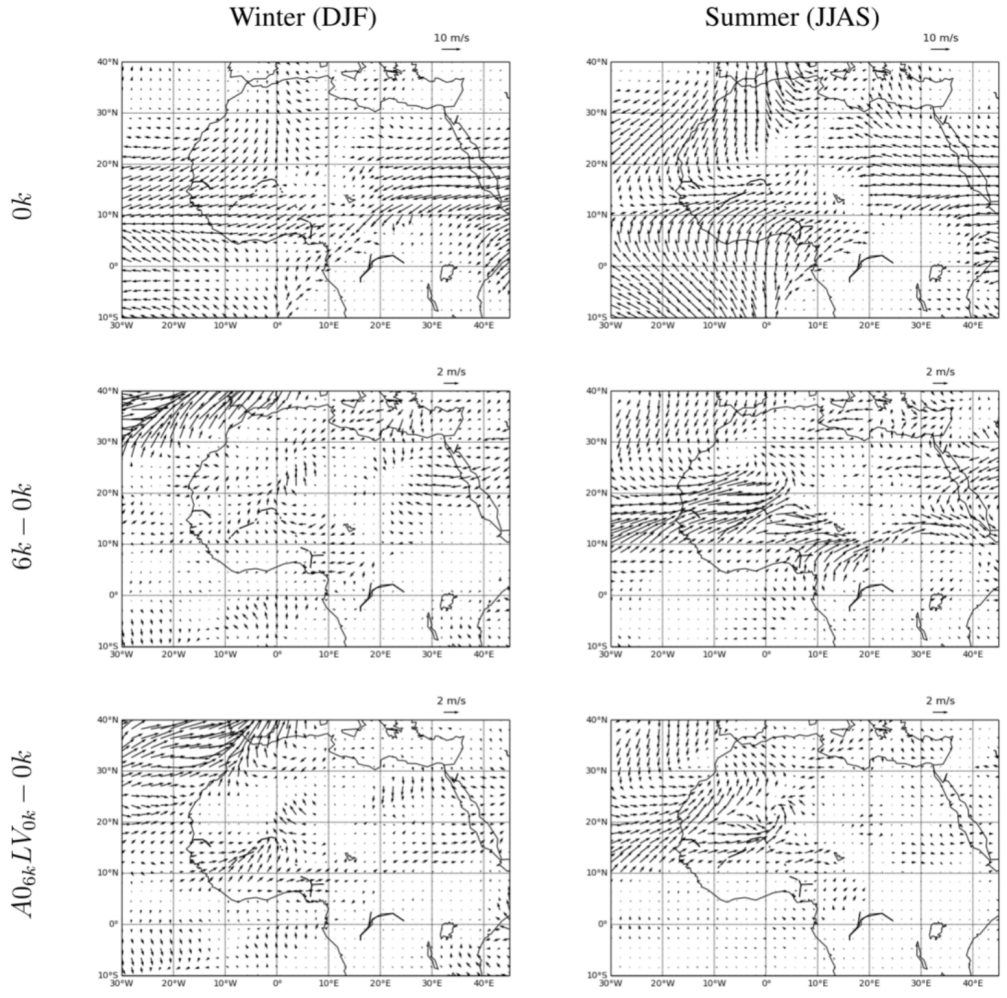

Figure 9. Simulated 10m surface wind speed and directions for winter (DJF; left) and summer (JJAS; right) for $0k$ and for the differences $6k - 0k$ and $A0_{6k}LV_{0k} - 0k$.

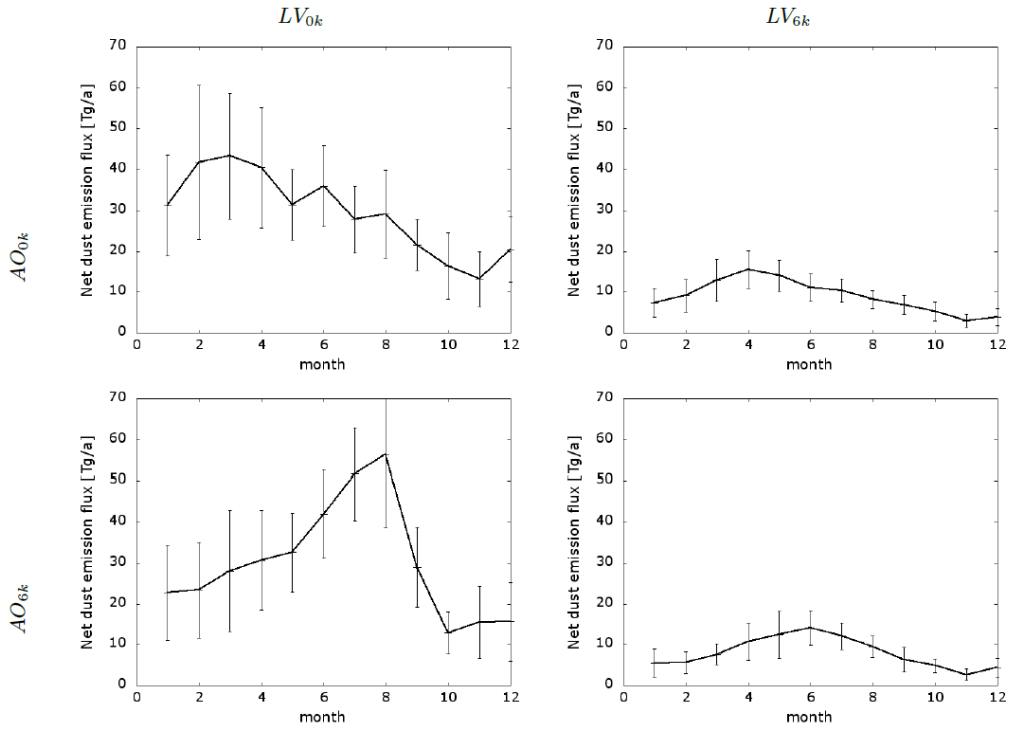

Figure 10. Mean annual cycle of simulated dust emission for altering atmosphere-ocean (AO) and land surface (LV) conditions in North Africa (17°W - 40°E; 10°N - 30°N)

.

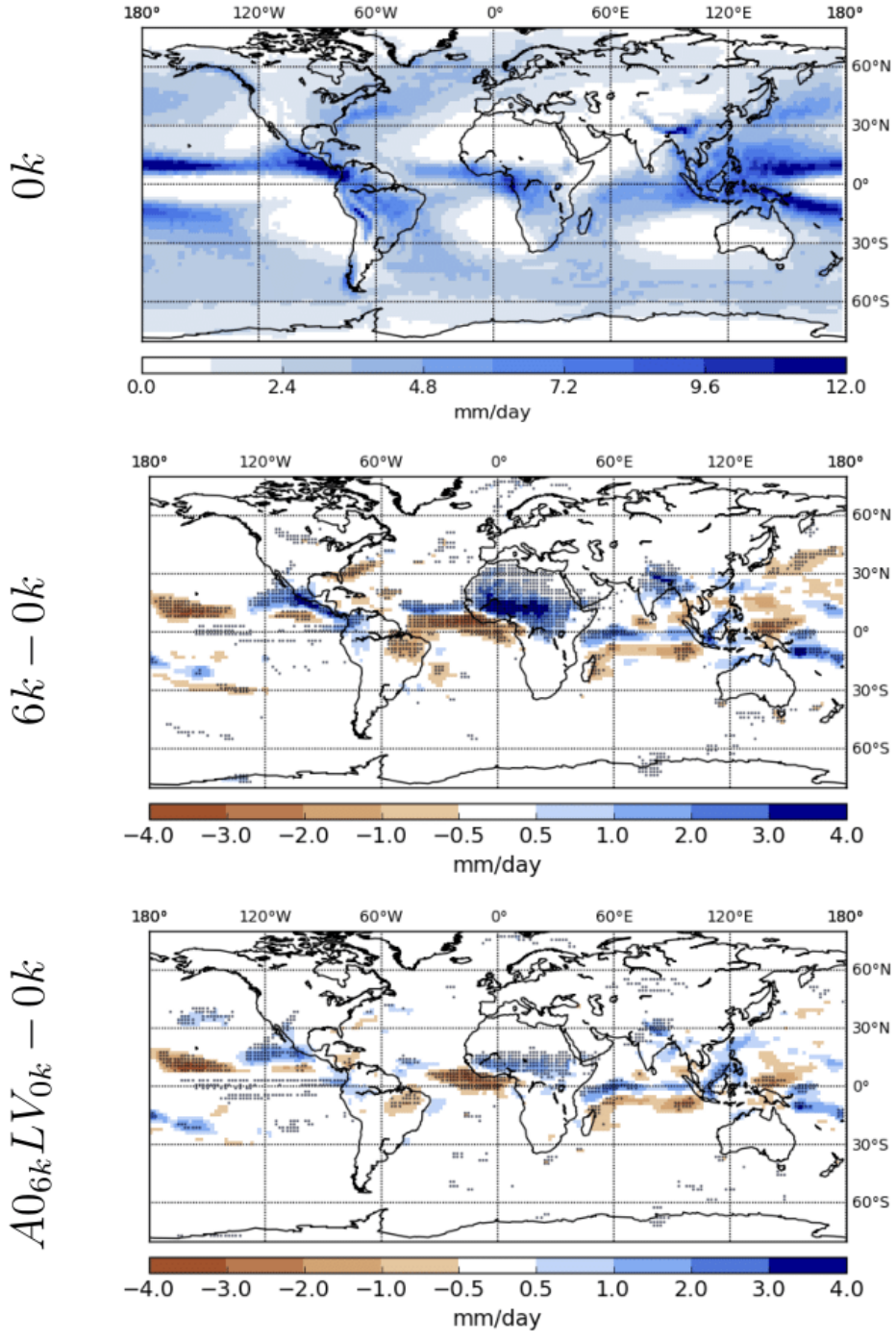

Figure 11. Mean annual precipitation for $0k$ and for the differences $6k - 0k$ and $A0_{6k}LV_{0k} - 0k$. Hatched areas in the difference plots show significant precipitation differences (99% confidence level) according to a Student's t test.

List of Tables

Model	Emission [Tga^{-1}]	Emission NA [Tga^{-1}]	Burden [Tg]	Wet Dep. [Tga^{-1}]	Dry Dep. [Tga^{-1}]	Sedi. [Tga^{-1}]
AEROCOM median (range)	1123 (514-4313)	792 (204-2888)	15.8 (6.8-29.5)	357 (295-1382)	396 (37-2791)	314 (22-2475)
ECHAM5-HAM (Stier et al., 2005)	664	401	8.28	374	37	265
ECHAM6.1-HAM2.1 (Stanelle et al., 2014)	912 $\pm$ 77	491 $\pm$ 66	10.9	473	83	358

Table 1. Global dust emission, burden and deposition, and emission in North Africa (NA) from the AEROCOM models (Huneeus et al., 2011) including ECHAM5-HAM for the year 2000 and from ECHAM6.1-HAM2.1 averaged for 2000-2009. Uncertainties in the last two rows are standard deviations of the 10 year ensemble.

	Orbit	SST, SIC	Lakes	Vegetation
$AO_{0k}LV_{0k}$	0k	0k	0k	0k
$AO_{0k}LV_{6k}$	0k	0k	6k	6k
$AO_{6k}LV_{0k}$	6k	6k	0k	0k
$AO_{6k}LV_{6k}$	6k	6k	6k	6k
$AO_{6k}L_{0k}V_{6k}$	6k	6k	0k	6k
$AO_{6k}L_{6k}V_{0k}$	6k	6k	6k	0k

Table 2. Experimental setup including orbital parameters, sea surface temperature (SST) and sea ice cover (SIC), lake and vegetation cover; $0k$ refers to pre-industrial and $6k$ to mid-Holocene conditions. While differences in AO conditions apply globally, differences in L and V conditions apply only to the Saharan box (17°W - 40°E; 10°N - 30°N).

	0k (pre-industrial)	**6k (mid-Holocene)**
Orbital parameters:		
Eccentricity	0.016715	0.018682
Obliquity ($^\circ$)	23.441	24.105
Precession ($^\circ$)	102.7	0.87
Greenhouse gases:		
CO_2 (ppm)	280	
CH_4 (ppb)	650	
N_2O (ppb)	270	

Table 3. Orbital parameters derived from Berger (1978) and greenhouse gas concentrations following the PMIP protocol for $6k$ (Harrison et al., 2001).

Marine sediment records							
No	Site	lat [°N]	lon [°E]	Dep. flux [$gm^{-2}a^{-1}$]			Reference
				$0k$	$6k$	$0k : 6k$	
1	ODP 659	18.1	-21.0	14.7			Tiedemann et al. (1989)
2	BOFS-1	19.0	-20.17	21.55			Bory and Newton (2000)
3	CB2-1	21.15	-20.68	19.7			Fischer et al. (1996)
4	CB2-2	21.15	-20.69	20.48			Ratmeyer et al. (1999)
5	CI 1 upper	29.11	-15.45	4.15			Ratmeyer et al. (1999)
6	22N25W	21.93	-25.23	6.7			Kremling and Streu (1993); Jickells et al. (1996)
7	25N23W	24.55	-22.83	5.21			Jickells et al. (1996)
8	28N22W	28.00	-21.98	2.4			Jickells et al. (1996)
9	GC 68	19.36	-17.28	22.0	4.1	5.4	McGee et al. (2013); Albani et al. (2015)
10	ODP 658C	20.75	-18.58	19.2	8.1	2.4	Adkins et al. (2006)
11	GC 49	23.21	-17.85	5.5	1.2	4.6	McGee et al. (2013); Albani et al. (2015)
12	GC 37	26.82	-15.12	3.4	0.92	3.7	McGee et al. (2013); Albani et al. (2015)

Table 4. Position, dust deposition fluxes for $0k$ and $6k$ and the corresponding flux ratio between $0k$ and $6k$ obtained from marine sediment cores (1, 9, 10, 11, 12) and sediment traps (2, 3, 4, 5, 6, 7, 8) close to the northwest African margin.

Simulated dust deposition flux close to site				
No	Site	Dep. flux [$gm^{-2}a^{-1}$]		
		$0k$	$6k$	$0k : 6k$
9	GC 68	18.5	6.0	3.1
10	ODP 658C	11.9	5.0	2.4
11	GC 49	8.3	3.7	2.3
12	GC 37	5.1	2.5	2.1

Table 5. Simulated dust deposition flux close to site GC68, ODP 658C, GC49 and GC37 (Table 4) for $0k$ and $6k$ and the corresponding flux ratios between $0k$ and $6k$.

Experiment	Emission [Tga^{-1}]	Burden [Tg]	Wet Dep. [%]	Dry Dep. [%]	Sedi. [%]	Total Dep. [Tga^{-1}]	Global life time [day]	Precip. [mm day^{-1}]
$AO_{0k}LV_{0k}$	352.6 $\pm$ 44.3	2.62	20.6	9.6	69.8	144.9	4.4	0.66
$AO_{6k}LV_{0k}$	360.5 $\pm$ 29.4	2.73	34.4	6.6	59.0	165.3	4.3	0.93
$AO_{0k}LV_{6k}$	107.8 $\pm$ 12.3	1.04	43.4	4.7	51.9	70.2	3.7	1.79
$AO_{6k}LV_{6k}$	96.1 $\pm$ 15.4	0.99	51.1	3.9	45.0	72.0	3.7	1.97
$AO_{6k}L_{0k}V_{6k}$	174.2 $\pm$ 28.8	1.69	47.2	3.2	49.6	100.9	4.1	1.72
$AO_{6k}L_{6k}V_{0k}$	177.7 $\pm$ 18.7	1.38	41.0	6.4	52.6	101.6	3.6	1.24

Table 6. Dust emission, burden, deposition and precipitation in North Africa (17°W - 40°E; 10°N - 30°N) and global life time of dust for altering atmospheric and ocean (AO) and land surface conditions (LV).

	Δ_{6k-0k} [Tga^{-1}]	$\Delta_{AO}/\Delta_{6k-0k}$	$\Delta_{LV}/\Delta_{6k-0k}$	$\Delta_{SYN}/\Delta_{6k-0k}$
Emission	-256.5	-3.1%	95.4%	7.6%
Deposition	-26.6	-16.5%	96.1%	20.4%

Table 7. Total difference in dust emission in North Africa (17°W - 40°E; 10°N - 30°N) and dust deposition along the northwest African margin (30°W - 17°W; 5°N - 35°N) between $6k$ and $0k$ and percentages of land surface conditions, atmosphere-ocean conditions and synergy effects to the total difference.